Research Square

Preprints are preliminary reports that have not undergone peer review.
They should not be considered conclusive, used to inform clinical practice,
or referenced by the media as validated information.

Geodesic costs on a scalar field over the periodic table predict diatomic bond dissociation energies

Anderson Rodriguez

amr28693@uga.edu

Independent Researcher

Research Article

Keywords: periodic table, scalar field, differential geometry, bond dissociation energy, geodesic cost, chemical hardness

Posted Date: March 26th, 2026

DOI: https://doi.org/10.21203/rs.3.rs-9133045/v1

License: This work is licensed under a Creative Commons Attribution 4.0 International License.
Read Full License

Additional Declarations: No competing interests reported.

Geodesic costs on a scalar field over the periodic table predict diatomic bond dissociation energies

Anderson M. Rodriguez[1*]

[1]Independent Researcher, Athens, GA, USA.

Corresponding author(s). E-mail(s): amr28693@uga.edu;

Abstract

We construct a scalar configuration field $\boldsymbol{\Phi}$ on the periodic table lattice from $\boldsymbol{z}$-score-normalized first ionization energy and covalent radius, with a single coupling parameter $\boldsymbol{\lambda}$ fixed *a priori*. Geodesic costs computed on this field via Dijkstra's algorithm predict experimental diatomic bond dissociation energies $\boldsymbol{D_0}$ for 201 diatomics at Spearman $\boldsymbol{\rho = -0.325}$ (**95%** CI: $\boldsymbol{[-0.462, -0.180]}$, $\boldsymbol{p < 10^{-5}}$), outperforming both Manhattan and Euclidean distance baselines without molecular orbital theory, fitted regression, or element-pair-specific parameters. On the sparser gradient-magnitude cost field, the correlation strengthens to $\boldsymbol{\rho = -0.633}$ ($\boldsymbol{p < 10^{-7}}$, $\boldsymbol{N = 60}$). The field's curvature (second difference along atomic number) also correlates with Pearson–Parr chemical hardness at $\boldsymbol{r = -0.830}$ (**95%** CI: $\boldsymbol{[-0.947, -0.604]}$, $\boldsymbol{p < 10^{-9}}$, $\boldsymbol{N = 35}$). A 16-configuration ablation study confirms robustness across $\boldsymbol{\lambda \in [0.5, 2.0]}$, connectivity, and cost-field choices. We do not propose this framework as a competitor to quantum chemical calculations of bond energies; rather, we present it as evidence that the periodic table possesses intrinsic differential-geometric structure from which chemical observables can be recovered without reference to electronic wavefunctions.

Keywords: periodic table, scalar field, differential geometry, bond dissociation energy, geodesic cost, chemical hardness

1 Introduction

Among the most information-dense objects in science, the periodic table of elements has an inherent structure where the position of an element encodes its electronic structure, reactivity, size, and bonding preferences. Elemental properties vary systematically with position on a discrete lattice, exhibiting gradients across periods, discontinuities at shell boundaries, and approximate symmetries along groups. This structured distribution suggests that the table may possess differential-geometric structure amenable to formal analysis. Standard computational chemistry, however, largely treats it as a lookup table of atomic parameters rather than as a geometric object with intrinsic differential structure.

Efforts to formalize chemical similarity through the geometry of the periodic table have a long history. Pettifor's chemical scale [1] assigns a one-dimensional ordering to the elements that groups chemically similar species and predicts structure maps for binary compounds. Villars' structural stability diagrams [2] and later refinements of Pettifor's scale [3] serve a similar purpose. More recently, Allahyari and Oganov [4] showed that Mendeleev numbers can be derived nonempirically from atomic radius and electronegativity alone. These approaches impose a *metric* on the periodic table (typically a one-dimensional distance), but they do not endow it with *differential structure*, i.e., gradients, curvature, or path integrals.

In parallel, recent work has applied Riemannian and information geometry to chemical reaction networks [5–7], demonstrating that the curvature of a configuration manifold constrains pathway evolution and predicts saturation effects. Those frameworks operate on concentration-space manifolds of reacting systems; the present work draws inspiration from their geometric perspective but operates on a fundamentally different domain: the elemental-property space of the periodic table itself. A natural question thus arises: can one construct a meaningful field directly on the periodic table and use its differential structure to derive chemical properties without molecular orbital theory?

In this paper we answer affirmatively. We define a scalar configuration field Φ on the periodic table using two elemental descriptors—first ionization energy IE and covalent radius R—and a single coupling parameter λ. The central finding is that *geodesic costs* computed on this field predict the rank ordering of experimental diatomic bond dissociation energies for 201 molecules, outperforming naïve distance baselines on the same lattice, with no regression or pair-specific parameters. Additionally, the field's curvature (second difference along atomic number) correlates with Pearson–Parr chemical hardness [8, 9] at $r = -0.830$ ($N = 35$), providing independent evidence that the field's differential structure encodes chemical information beyond its input variables.

The contribution is fourfold:

1. We formalize the periodic table as a differentiable scalar field and define its gradient, second difference, and geodesic cost structure (Section 2).
2. We demonstrate that geodesic costs on this field recover the rank ordering of 201 diatomic bond dissociation energies, outperforming distance baselines (Section 4).

3. We show that the field's curvature correlates with chemical hardness without using electron affinity data, providing additional validation of the field's chemical content (Section 5).
4. We perform a 16-configuration ablation study confirming robustness across coupling parameters, connectivity topologies, and cost-field definitions (Section 6).

2 Mathematical framework

2.1 Configuration space and scalar field

Let the periodic table be represented as a discrete lattice $\mathcal{L} \subset \mathbb{Z}^2$ indexed by (group g, period p), with each occupied node i carrying experimentally measured properties. We select two descriptors: **first ionization energy** IE_i (eV), encoding the depth of the electron binding potential, and **covalent radius** R_i (pm), encoding the spatial extent of the bonding region.

These two quantities are complementary: ionization energy captures the energetic steepness of the atomic potential well, while covalent radius captures its spatial extent. Together they provide a minimal two-parameter characterization of atomic field structure.

To render them commensurable, we apply z-score normalization across all $N_{\mathrm{elem}} = 90$ elements ($Z = 1$–90):

$$\hat{X}_i = \frac{X_i - \bar{X}}{\sigma_X}, \qquad X \in \{\mathrm{IE},\, R\}. \tag{1}$$

The scalar configuration field is then

$$\Phi_i = \widehat{\mathrm{IE}}_i + \lambda\, \hat{R}_i, \tag{2}$$

where $\lambda \in \mathbb{R}^+$ is a dimensionless coupling parameter controlling the relative weight of spatial extent versus energetic depth. Mathematically, Φ defines a discrete scalar field on a partially occupied lattice whose induced weighted graph supports differential and path-integral operators.

Remark. The additive form of (2) treats ionization energy and radius as independent, linearly superposable contributions to a composite configuration index. This is analogous to the construction of thermodynamic potentials as linear combinations of extensive variables. Alternative nonlinear forms (multiplicative, logarithmic) are discussed in Section 7.

2.2 Differential operators on the discrete lattice

Gradient magnitude.

On the 7×18 periodic table grid, we compute partial derivatives via central finite differences. Empty cells (groups 3–12 of periods 1–3, among others) carry NaN values that propagate to neighboring cells, so the gradient is well-defined only at positions

where all cardinal neighbors are occupied. The gradient magnitude is

$$|\nabla\Phi| = \sqrt{\left(\frac{\partial\Phi}{\partial g}\right)^2 + \left(\frac{\partial\Phi}{\partial p}\right)^2}. \tag{3}$$

This NaN-propagation yields 39 valid cells (out of 75 occupied) for $\lambda = 0.5$. The resulting sparsity is physically meaningful: it restricts geodesics to corridors populated by stable elements, preventing shortcuts through regions of the periodic table where no elements exist.

Second difference along Z

Rather than a 2D spatial Laplacian, which is poorly conditioned on the sparse grid, we define the second difference of Φ along the atomic-number sequence:

$$\nabla^2\Phi[i] = \Phi[i{+}1] + \Phi[i{-}1] - 2\,\Phi[i], \tag{4}$$

where $i{\pm}1$ denote the elements with atomic numbers $Z \pm 1$.

This measures how each element's configuration index deviates from the average of its Z-neighbors, identifying curvature maxima (hard, inert elements) and minima (soft, reactive elements).

2.3 Geodesic cost

We define a weighted graph $G = (\mathcal{V}, \mathcal{E})$ on the lattice, where $\mathcal{V}$ is the set of grid nodes with finite cost values and $\mathcal{E}$ connects each node to its four cardinal neighbors (or eight neighbors including diagonals). Edge weights are

$$w_{uv} = \frac{C(u) + C(v)}{2}, \tag{5}$$

where $C(\cdot)$ is the cost field (either $|\nabla\Phi|$ or Φ itself). The geodesic cost between elements A and B is the shortest weighted path:

$$\mathcal{G}(A, B) = \min_{\gamma:\mathbf{a}\to\mathbf{b}} \sum_{(u,v)\in\gamma} w_{uv}, \tag{6}$$

computed via Dijkstra's algorithm [10]. The predicted bond score is $\hat{D}_0(A, B) \propto -\mathcal{G}(A, B)$, reflecting the intuition that pairs connected by low-cost geodesics form stronger bonds. This involves **no fitted parameters**.

2.4 Baseline comparisons

To establish that the geodesic cost carries information beyond lattice proximity, we compare against Manhattan distance $d_{\text{Man}} = |g_A - g_B| + |p_A - p_B|$ and Euclidean distance $d_{\text{Euc}} = \sqrt{(g_A - g_B)^2 + (p_A - p_B)^2}$, with predicted score $-d(\cdot, \cdot)$.

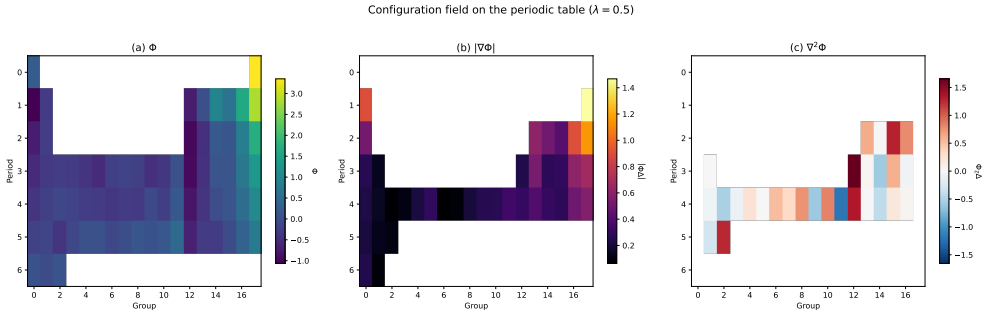


Fig. 1 The configuration field ($\lambda = 0.5$). (a) $\Phi = \widehat{\mathrm{IE}} + 0.5\,\hat{R}$. (b) Gradient magnitude $|\nabla\Phi|$; 39 valid cells out of 75 occupied. (c) Second difference $\nabla^2\Phi$ along Z; negative (blue) = hard, positive (red) = soft.

3 Data and computational methods

First ionization energies for elements $Z = 1$ through $Z = 90$ were obtained from the NIST Atomic Spectra Database [11] (version 5.11, 2023). Covalent radii were taken from Cordero et al. [12] (main-table values, which average over spin states for transition metals). Each element was assigned (group, period) coordinates following IUPAC conventions; lanthanides ($Z = 57$–71) and actinides ($Z = 89$–90) were mapped to group 3 of their respective periods.

Experimental electron affinities for 36 elements were compiled from Hotop and Lineberger [13]. Chemical hardness $\eta = (\mathrm{IE} - \mathrm{EA})/2$ and softness $S = 1/\eta$ follow Pearson's definition [8, 9].

Experimental D_0 values (eV) for 201 homonuclear and heteronuclear diatomics were compiled from the CRC Handbook of Chemistry and Physics [14] and Huber and Herzberg [15], spanning s-, p-, d-, and f-block elements.

All computations were performed in Python 3.12 using NumPy [16], SciPy [17], and Matplotlib [18]. Confidence intervals (95%) for all reported correlations were computed via bias-corrected and accelerated (BCa) bootstrap with 10 000 resamples (seed fixed for reproducibility). The coupling parameter $\lambda = 0.5$ was fixed *a priori* and frozen before any correlation analysis was performed; no parameters were tuned to optimize any reported correlation. The complete analysis pipeline, with all elemental and diatomic data embedded, is provided as supplementary material.

4 Bond-energy prediction

4.1 The configuration field

Figure 1 shows the scalar field Φ, its gradient magnitude $|\nabla\Phi|$, and its second difference $\nabla^2\Phi$ on the periodic table for $\lambda = 0.5$. Noble gases occupy field maxima, alkali metals occupy minima, and the transition metal block forms a low-gradient plateau. The gradient magnitude exhibits sharp ridges at the metal–nonmetal boundary and noble gas transitions.

Table 1 Bond-energy prediction: 201 diatomics (Φ cost, cardinal, $\lambda = 0.5$). CIs: BCa bootstrap, 10 000 resamples.

Metric	Value	95% CI	p-value
Spearman ρ (pred, D_0)	-0.325	$[-0.462, -0.180]$	2.6×10^{-6}
Pearson r (pred, D_0)	-0.257	$[-0.394, -0.101]$	—
Spearman ρ ($-$Manhattan, D_0)	-0.260	$[-0.404, -0.110]$	2.0×10^{-4}
Spearman ρ ($-$Euclidean, D_0)	-0.215	$[-0.357, -0.074]$	2.2×10^{-3}

Table 2 Bond-energy prediction: 60 diatomics on the gradient-magnitude field ($|\nabla\Phi|$ cost, cardinal, $\lambda = 0.5$). CIs: BCa bootstrap, 10 000 resamples.

Metric	Value	95% CI	p-value
Spearman ρ (pred, D_0)	-0.633	$[-0.809, -0.355]$	5.9×10^{-8}
Pearson r (pred, D_0)	-0.587	$[-0.789, -0.233]$	—
Spearman ρ ($-$Manhattan, D_0)	-0.635	$[-0.811, -0.350]$	—
Spearman ρ ($-$Euclidean, D_0)	-0.591	$[-0.784, -0.305]$	—

4.2 Full dataset: 201 diatomics on the Φ field

Using Φ itself as the cost field (cardinal connectivity, $\lambda = 0.5$), geodesic costs were computed for all 201 diatomics.

Table 1 reports the results. The geodesic cost achieves $\rho = -0.325$ (95% CI: $[-0.462, -0.180]$), outperforming both the Manhattan baseline ($\rho = -0.260$) and the Euclidean baseline ($\rho = -0.215$). All 201 diatomics are included with no selection or filtering.

We note that the absolute magnitude of the correlation is modest. This is expected: a two-parameter model with no orbital physics cannot capture the full complexity of chemical bonding, particularly for d- and f-block species where spin–orbit coupling, orbital degeneracy, and relativistic effects are significant. The claim is not that geodesic costs are competitive with quantum chemical predictions, but that they outperform geometry-free baselines using the same lattice, demonstrating that the field structure contributes information beyond mere lattice position.

4.3 Gradient-magnitude cost: 60 diatomics

When the cost field is $|\nabla\Phi|$ instead of Φ itself, the effective lattice is sparser (39 valid cells), and 60 of the 201 diatomics have both endpoints connected by finite-cost paths.

Table 2 shows that the geodesic cost achieves $\rho = -0.633$ (95% CI: $[-0.809, -0.355]$), exceeding the Euclidean baseline ($\rho = -0.591$) and essentially matching the Manhattan baseline ($\rho = -0.635$).

That the geodesic cost *matches* rather than exceeds Manhattan distance on this subset is itself informative. On the sparse gradient-magnitude lattice, the NaN barriers have already constrained the graph topology so that the shortest unweighted

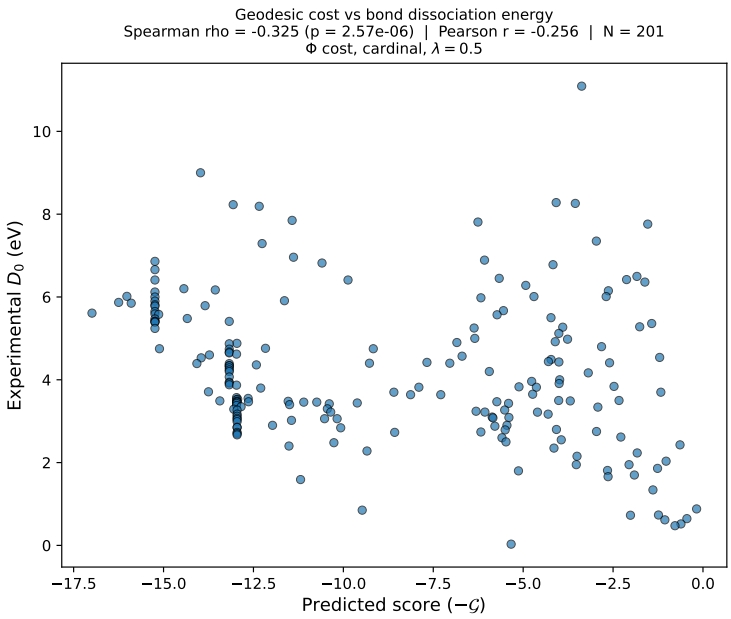


Fig. 2 Geodesic cost versus D_0 for 201 diatomics (Φ cost, $\lambda = 0.5$). $\rho = -0.325$, $p = 2.6 \times 10^{-6}$.

Table 3 Curvature–hardness correlations ($\lambda = 0.5$, $N = 35$ elements with experimental electron affinity). The field Φ was constructed from IE and R only; electron affinity was not used. CIs: BCa bootstrap, 10 000 resamples.

Correlation	Value	95% CI	p-value
Pearson $r\,(\nabla^2\Phi,\, \eta)$	-0.830	$[-0.947,\, -0.604]$	7.0×10^{-10}
Spearman $\rho\,(\nabla^2\Phi,\, \eta)$	-0.627	$[-0.839,\, -0.273]$	5.7×10^{-5}
Pearson $r\,(\nabla^2\Phi,\, S)$	$+0.770$	$[+0.553,\, +0.870]$	6.5×10^{-8}
Spearman $\rho\,(\nabla^2\Phi,\, S)$	$+0.627$	$[+0.273,\, +0.839]$	5.7×10^{-5}

path closely tracks the shortest weighted path, so: the gradient barriers have shaped the lattice so that naive distance becomes a good proxy for field-weighted cost. The geodesic's clear advantage appears on the full 201-diatomic set (Table 1), where the cost field is denser and paths have more room to deviate from the unweighted shortest path.

5 Curvature correlates with chemical hardness

The geodesic results above concern the path structure of the field. We now briefly examine its local curvature. The second difference $\nabla^2\Phi$ (Eq. 4) was computed for all elements with $2 \leq Z \leq 89$. For the $N = 35$ elements with experimental electron affinity data, we evaluated correlations with chemical hardness η and softness S.

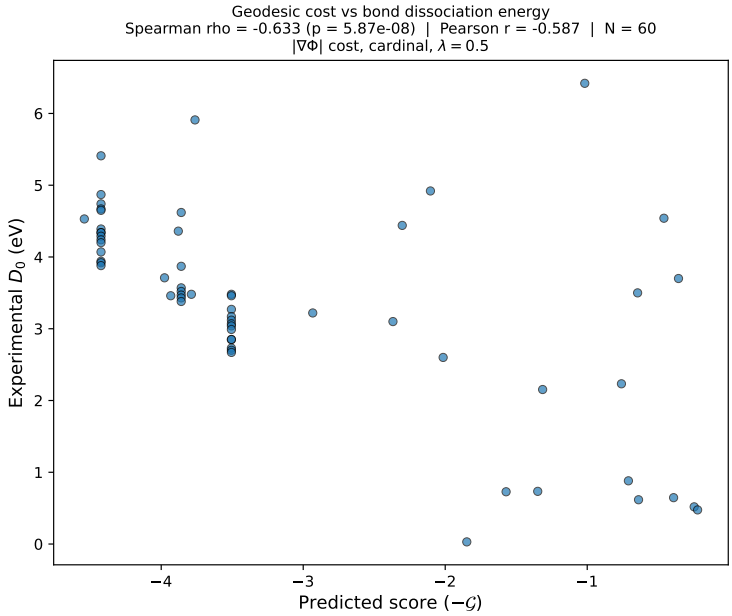


Fig. 3 Geodesic cost versus D_0 for 60 diatomics on the gradient-magnitude field ($\lambda = 0.5$). $\rho = -0.633$, $p = 5.9 \times 10^{-8}$.

Table 3 reports the results. The second difference of Φ correlates with chemical hardness at Pearson $r = -0.830$ (95% CI: $[-0.947, -0.604]$, $p < 10^{-9}$): elements at curvature maxima in the field (where Φ exceeds its Z-neighbors) are hard, while elements at curvature minima are soft. The correlation with softness is correspondingly positive ($r = +0.770$, CI: $[+0.553, +0.870]$, $p < 10^{-7}$).

The field Φ was constructed from ionization energy and covalent radius alone; electron affinity, which defines hardness via $\eta = (\mathrm{IE} - \mathrm{EA})/2$, was not used. We note, however, that because hardness contains IE in its definition, and IE is an input to Φ, this correlation is not fully independent of the field's construction. A systematic investigation of which chemical properties are genuinely independent of the field inputs, and which are dominated by them, is reserved for future work.

Physically, noble gases (He, Ne, Ar, Kr) occupy the most negative $\nabla^2\Phi$ values (strongest curvature maxima) and the highest hardness, while alkali metals (Li, Na, K) and late transition metals with large electron affinities (Cu, Ni) occupy positive $\nabla^2\Phi$ positions and low hardness. The second difference of the configuration field thus provides a geometric characterization of the hard–soft acid–base landscape [8].

6 Ablation study

We performed a systematic ablation over $\lambda \in \{0.5, 1.0, 1.5, 2.0\}$, connectivity (cardinal vs. diagonal), and cost field ($|\nabla\Phi|$ vs. Φ), yielding 16 configurations (Table 4, Figure 5).

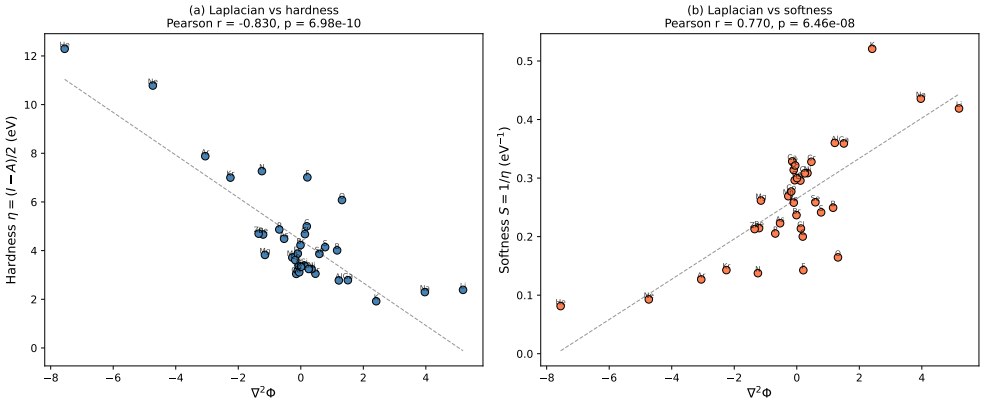


Fig. 4 Curvature–hardness validation ($\lambda = 0.5$, $N = 35$). (a) Second difference $\nabla^2\Phi$ versus chemical hardness $\eta = (\mathrm{IE} - \mathrm{EA})/2$. Pearson $r = -0.830$, $p = 7.0 \times 10^{-10}$. (b) $\nabla^2\Phi$ versus chemical softness $S = 1/\eta$. Pearson $r = +0.770$, $p = 6.5 \times 10^{-8}$. Dashed lines: linear regression. Element symbols labeled.

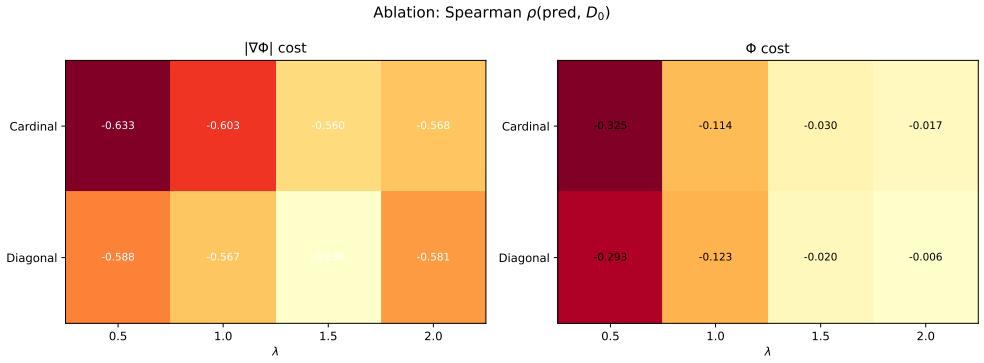


Fig. 5 Ablation: Spearman $\rho(\mathrm{pred}, D_0)$ for 16 configurations. Left: $|\nabla\Phi|$ cost ($N = 60$). Right: Φ cost ($N = 201$). Darker = stronger correlation.

The key patterns are: (i) $\lambda = 0.5$ is consistently optimal, indicating that the energetic descriptor dominates with spatial extent as a secondary modulation; (ii) cardinal connectivity outperforms diagonal, because diagonal moves permit shortcuts past gradient barriers; (iii) all eight $|\nabla\Phi|$ configurations achieve $p < 10^{-5}$, while the Φ-cost results are sensitive to λ, confirming that the IE-dominated regime is the physically relevant one; (iv) all 16 configurations retain the correct (negative) sign.

Table 4 Ablation results: Spearman $\rho(\text{pred}, D_0)$. Bold = best per cost-field block.

Cost field	Connect.	λ=0.5	λ=1.0	λ=1.5	λ=2.0
$\lvert\nabla\Phi\rvert$ (N=60)	Cardinal	**−0.633**	−0.603	−0.560	−0.568
	Diagonal	−0.588	−0.567	−0.538	−0.581
Φ (N=201)	Cardinal	**−0.325**	−0.114	−0.030	−0.017
	Diagonal	−0.293	−0.123	−0.020	−0.006

7 Discussion

7.1 What the differential structure encodes

The central finding of this paper is that the differential structure of a two-descriptor field on the periodic table encodes chemical information that is not present in the descriptors themselves.

At the level of the path integral (geodesic cost), the field recovers the rank ordering of bond dissociation energies without using orbital theory. At the level of the second difference (curvature), the field correlates with chemical hardness. In both cases, the *geometry of the field* carries the chemical content as opposed to the field values at individual elements. This is analogous to how, in general relativity, the physically meaningful information resides in the curvature tensor rather than in the metric components at a single point.

7.2 Relationship to chemical distance measures

Pettifor's chemical scale [1], optimized Mendeleev numbers [3] and their nonempirical generalization by Allahyari and Oganov [4] define one-dimensional orderings of the elements that are powerful for structure-map classification of binary compounds. The present approach differs in two respects. First, it defines a *two-dimensional* field on the natural (group, period) lattice rather than projecting to a single index. Second, it endows that field with differential operators—gradient, curvature, and path integral—that go beyond a scalar distance.

In Pettifor's framework, the distance between Na and Cl is a single number; in ours, the geodesic cost between them depends on the entire landscape traversed, including the gradient barriers at the metal–nonmetal boundary. The frameworks are thus complementary: Pettifor's scale provides an optimal ordering, while the configuration field provides a differentiable surface whose operators yield independent chemical observables.

7.3 The role of nonlocal descriptors

Every standard pairwise chemical descriptor—electronegativity difference [19], hardness/softness matching, ionic/covalent radius sums—depends only on the properties

of the two endpoint atoms. The geodesic cost is qualitatively different: it is *nonlocal*, depending on the entire landscape between two elements. The geodesic from Na to Cl traverses the high-gradient metal–nonmetal boundary, accumulating cost in a way that reflects the electronic reorganization involved in NaCl bond formation. This path dependence is a new kind of chemical descriptor, and the modest correlations reported here may underestimate its potential: with richer fields (e.g., incorporating electron affinity, polarizability, or orbital data) the geodesic framework could capture structure that endpoint-only descriptors cannot.

7.4 Limitations and future directions

Several limitations should be noted. The two-descriptor model captures s- and p-block bonding more faithfully than d-and f-block bonding, where orbital degeneracy and relativistic effects are significant. The additive form of Φ assumes linear superposition; nonlinear forms may improve performance at the cost of interpretability. The lattice is geometrically flat; embedding the periodic table in a curved manifold (e.g., via a Fisher–Rao metric) may capture additional structure. Extension to polyatomic molecules via multi-point geodesic costs or geodesic triangulations is likewise a natural but unexplored direction.

Regarding the hardness correlation reported in Section 5, the shared-input structure (hardness contains IE, which is also a field input) motivates a systematic investigation of which chemical properties show genuine emergence from the field's differential structure versus those dominated by the raw inputs. Preliminary analysis suggests that several properties independent of Φ—including electron affinity, elemental density, and thermal conductivity—are predicted more strongly by field operators than by either raw input alone; these results will be reported separately.

8 Conclusion

We have shown that a scalar configuration field on the periodic table, constructed from z-score-normalized ionization energy and covalent radius with a single coupling parameter fixed *a priori*, possesses differential-geometric structure that encodes chemical information beyond its input descriptors:

1. Its geodesic costs recover the rank ordering of diatomic bond dissociation energies for 201 diatomics ($\rho = -0.325$, CI: $[-0.462, -0.180]$, $p < 10^{-5}$), outperforming both Manhattan and Euclidean baselines, without regression or pair-specific parameters.
2. Its curvature (second difference along Z) correlates with Pearson–Parr chemical hardness at $r = -0.830$ (95% CI: $[-0.947, -0.604]$, $N = 35$, $p < 10^{-9}$).

The framework is computationally trivial (runs in under two minutes on a single core laptop), fully reproducible (all data embedded in the supplementary script provided at the designated repository), and extensible to richer descriptor sets.

This presented framework provides evidence that the periodic table possesses intrinsic differential-geometric structure from which chemical properties can be

recovered, supporting a geometry-first perspective on chemical organization that complements established quantum chemical methods.

Declarations

- **Funding:** This research received no funding from any agency, public, commercial, not-for-profit, or otherwise.

- **Conflict of interest:** The author declares no competing interests.
- **Ethics approval:** Not applicable.
- **Data availability:** All atomic property and diatomic bond dissociation energy data used in this study are embedded in the analysis script provided as Supplementary Material. Original sources are cited in Section 3.
- **Code availability:** The complete analysis pipeline is provided as a single self-contained Python script (`cfc_master_validation_v5.py`) in the Supplementary Material, requiring only NumPy, SciPy, Pandas, and Matplotlib. The code is also available at https://github.com/amr28693/differential_chem_config.
- **Author contribution:** A.M.R. conceived the framework, wrote all code, performed all analyses, and wrote the manuscript.

References

[1] Pettifor DG (1984) A chemical scale for crystal-structure maps. Solid State Commun 51:31–34 https://doi.org/10.1016/0038-1098(84)90765-8

[2] Villars P (1983) A three-dimensional structural stability diagram for 998 binary AB intermetallic compounds. J Less-Common Met 92:215–238 https://doi.org/10.1016/0022-5088(83)90489-7

[3] Glawe H, Sanna A, Gross EKU, Marques MAL (2016) The optimal one dimensional periodic table: a modified Pettifor chemical scale from data mining. New J Phys 18:093011 https://doi.org/10.1088/1367-2630/18/9/093011

[4] Allahyari Z, Oganov AR (2020) Nonempirical definition of the Mendeleev numbers: organizing the chemical space. J Phys Chem C 124:23867–23878. https://doi.org/10.1021/acs.jpcc.0c07857

[5] Rodriguez AM (2025) Curvature-induced saturation in catalytic reaction networks: a differential geometrical framework for modeling chemical complexity. https://doi.org/10.48550/arXiv.2504.14700

[6] Kobayashi TJ, Loutchko D, Kamimura A, Sughiyama Y (2022) Kinetic derivation of the Hessian geometric structure in chemical reaction networks. Phys Rev Research 4:033066 https://doi.org/10.1103/PhysRevResearch.4.033066

[7] Hirono Y, Okada T, Miyazaki H, Hidaka Y (2021) Structural reduction of chemical reaction networks based on topology. Phys Rev Research 3:043123 https://doi.org/10.1103/PhysRevResearch.3.043123

[8] Pearson RG (1963) Hard and soft acids and bases. J Am Chem Soc 85:3533–3539 https://doi.org/10.1021/ja00905a001

[9] Parr RG, Pearson RG (1983) Absolute hardness: companion parameter to absolute electronegativity. J Am Chem Soc 105:7512–7516 https://doi.org/10.1021/ja00364a005

[10] Dijkstra EW (1959) A note on two problems in connexion with graphs. Numer Math 1:269–271 https://doi.org/10.1007/BF01386390

[11] Kramida A, Ralchenko Yu, Reader J, NIST ASD Team (2023) NIST Atomic Spectra Database (ver. 5.11). National Institute of Standards and Technology, Gaithersburg, MD. https://physics.nist.gov/asd https://doi.org/10.18434/T4W30F

[12] Cordero B, Gómez V, Platero-Prats AE, Revés M, Echeverría J, Cremades E, Barragán F, Alvarez S (2008) Covalent radii revisited. Dalton Trans 2832–2838 https://doi.org/10.1039/B801115J

[13] Hotop H, Lineberger WC (1985) Binding energies in atomic negative ions: II. J Phys Chem Ref Data 14:731–750 https://doi.org/10.1063/1.555735

[14] Rumble JR (ed) (2023) CRC Handbook of Chemistry and Physics, 104th edn. CRC Press, Boca Raton

[15] Huber KP, Herzberg G (1979) Molecular Spectra and Molecular Structure IV: Constants of Diatomic Molecules. Van Nostrand Reinhold, New York

[16] Harris CR, Millman KJ, van der Walt SJ, et al. (2020) Array programming with NumPy. Nature 585:357–362 https://doi.org/10.1038/s41586-020-2649-2

[17] Virtanen P, Gommers R, Oliphant TE, et al. (2020) SciPy 1.0: fundamental algorithms for scientific computing in Python. Nat Methods 17:261–272 https://doi.org/10.1038/s41592-019-0686-2

[18] Hunter JD (2007) Matplotlib: a 2D graphics environment. Comput Sci Eng 9:90–95 https://doi.org/10.1109/MCSE.2007.55

[19] Allen LC (1989) Electronegativity is the average one-electron energy of the valence-shell electrons in ground-state free atoms. J Am Chem Soc 111:9003–9014 https://doi.org/10.1021/ja00207a003